DESIGN OPTIMIZATION OF DEEPDRAWING PROCESS

Kyung K. Choi [*] ***and Nam H. Kim*** [¶]

The Center for Computer-Aided Design
and Department of Mechanical Engineering
College of Engineering
The University of Iowa
Iowa City, IA52242

ABSTRACT

The design optimization of deepdrawing process in manufacturing is proposed to control the final shape of the workpiece after elastic springback. The manufacturing process design problem is formulated to minimize the difference between the shape of the desired workpiece geometry and the final analysis result after elastic springback. Nonlinear structural problem that includes elastoplasticity with frictional contact is solved using a meshfree method where the structural domain is discretized by a set of particle points. Continuum-based design sensitivity analysis (DSA) is carried out to efficiently obtain the gradient information for the optimization. The shape of the workpiece and the geometry of the rigid die are treated as design variables. The accuracy of the sensitivity result is compared with the finite difference result with excellent agreement. The optimum stamping process improves the quality of the final product significantly.

1. INTRODUCTION

In spite of the significant developments of analysis and design capabilities in modern technology, there still remains gap between the simulation-based design and manufacturing process. Two major reasons are lack of efficient and accurate numerical methods for the design process. First, accurate numerical method has to be used to simulate manufacturing processes that include large deformation, complicate constitutive relation, and sliding contact between the workpiece and die. Second, efficient numerical methods have to be used to make the stamping optimization process practical. It is the purpose of this paper to demonstrate that these two obstacles can be resolved by using accurate numerical methods and efficient DSA.

In this paper, the design optimization of a deepdrawing process in manufacturing is proposed to control the final shape of the workpiece after elastic springback. The manufacturing process design problem is formulated to minimize the difference between the shape of the desired workpiece geometry and final analysis result after elastic springback. The amount of plastic strain and the reduction of workpiece thickness are design constraints so that the material separation and distortion can be prevented. The design parameters can be chosen from the thickness of the workpiece, the geometry of the die and punch, the frictional coefficient between contact surfaces, and the binder force to effectively control the output of the manufacturing process. Accurate sensitivity information of the cost and constraint functions with respects to design parameters play a critical role in effective design optimization. An important feature of this paper is to calculate the design sensitivity information accurately and efficiently when the workpiece experiences finite elasto-plastic deformation with complicate frictional contact constraints.

A continuum-based shape design sensitivity formulation is proposed for finite deformation elasto-plasticity with frictional contact. For response analysis, the multiplicative decomposition of the deformation gradient into elastic and plastic parts is used for the hyperelastic based plasticity constitutive model with respect to the intermediate configuration. The classical return-mapping algorithm of the small deformation plasticity theory is preserved and the tangent operator has the same form as the algorithmic tangent operator of the infinitesimal theory by using the principal space of the Kirchhoff stress and logarithmic strain tensors. For shape design sensitivity, the shape variation is taken with respect to the undeformed geometry of the workpiece, die, and punch. For sizing design sensitivity, variations with respect to the binder force and frictional coefficient are taken. The path-dependency of the sensitivity formulation comes from the evolution of the intermediate configuration and the internal plasticity variables as well as the frictional effect in contact constraint. Numerical examples show the accuracy and

* Professor and Director, Associate Fellow AIAA
¶ Postdoctoral Associates, Member AIAA

efficiency of the computation of design sensitivity information, compared with the finite difference results.

When a structure experiences a finite deformation, the conventional finite element method may have a difficulty in response analysis due to mesh distortion. The mesh regeneration may not be an effective approach to resolve this difficulty. In addition, for shape design problems, mesh distortion is a major concern due to large shape design perturbations. An effective numerical method, which can handle finite deformation, is highly desirable for both nonlinear analysis and shape optimization. The meshfree method is an ideal choice since, unlike the conventional finite element method, the solution is much less sensitive to mesh distortion. In the meshfree method, the structural domain is discretized with a finite number of particles whereas, in the finite element method, it is discretized with elements. The shape function at a point of discretized domain is constructed based on a set of scatter particles around the point and using modified kernel functions that are constructed by enforcing the reproducing conditions so that the kernel estimates of displacement variables exactly reproduces certain class of polynomials. In this paper, meshfree analysis is used to solve the nonlinear response problem and, thus design sensitivity analysis and manufacturing process optimization.

2. DEEPDRAWING ANALYSIS

The deepdrawing process involves a large amount of plastic deformations and rigid body rotations as well as complicate contact between the workpiece and die. Many simplified approaches are proposed to simulate the metal forming process. One major trend is ignoring the elastic deformation of the structure compared to the plastic part. Antunez (1996), Maniatty (1996), Zhao (1997), Chung (1998), and Balagangadhar (1998) used rigid-plasticity formulation to solve the metal forming design problems. This approach is meaningful for bulk metal forging type problems. As shown in Section 4, however, the elastic spring-back at the end of deepdrawing process plays a key role to the quality of the final products. Thus, the constitutive relation that counts the elastic and plastic properties together has to be used in practice.

Elastoplasticity in Finite Deformation

The classical theory of elasto-plasticity assumes the additive decomposition of the elastic and plastic strains. However, small deformation and small rigid body rotation is behind this theory. Even if many researches on the objective rate were carried out, the question remains about the numerical integration methods for the objective rate, which satisfy all the physical requirements. The difficulty of obtaining an exact tangent stiffness operator causes error in DSA and this error is accumulating as the analysis progresses. In this paper, kinematics proposed by Lee (1969) is used where the deformation gradient $\mathbf{F}(\mathbf{X}) = \partial\mathbf{x}/\partial\mathbf{X}$ is decomposed multiplicatively into elastic and plastic parts.

$$\boldsymbol{F}(\boldsymbol{X}) = \boldsymbol{F}^{e}(\boldsymbol{X})\boldsymbol{F}^{p}(\boldsymbol{X}) \tag{1}$$

where $\mathbf{F}^p(\mathbf{X})$ denotes the deformation through the intermediate configuration, which is related to the internal variables, and $\mathbf{F}^{e-1}(\mathbf{X})$ defines the local, stress-free, unloaded process. The stress-strain relation is given as a hyper-elasticity between the intermediate and the current configurations. The computational framework of this theory is proposed by Simo (1992), that preserves the conventional return-mapping algorithm in the principal stress space.

By using the principle of virtual work, the structural problem is formulated in a weak form to find the displacement $\mathbf{z}$ that satisfies

$$a_{\Omega}(\mathbf{z},\bar{\mathbf{z}}) = \ell_{\Omega}(\bar{\mathbf{z}}), \qquad \forall\bar{\mathbf{z}} \in Z \tag{2}$$

where Z is the space of the kinematically admissible displacements, that satisfies the essential boundary conditions. Equation (2) contains finite deformation including elasto-plasticity and rigid body rotation. In Eq. (2), $a_{\Omega}(\mathbf{z},\bar{\mathbf{z}})$ and $\ell_{\Omega}(\bar{\mathbf{z}})$ are the structural energy and load forms, respectively, defined as

$$a_{\Omega}(\mathbf{z},\bar{\mathbf{z}}) = \iint_{\Omega} \tau_{ij}\varepsilon_{ij}(\bar{\mathbf{z}})\,d\Omega \tag{3}$$

$$\ell_{\Omega}(\bar{\mathbf{z}}) = \iint_{\Omega} \bar{\mathbf{z}}^{T}\mathbf{f}^{b}\,d\Omega + \int_{\Gamma^{h}} \bar{\mathbf{z}}^{T}\mathbf{f}^{h}\,d\Gamma \tag{4}$$

where τ_{ij} is the Kirchhoff stress tensor, ε_{ij} the engineering strain at the current configuration, $\mathbf{f}^b$ the body force per unit volume, and $\mathbf{f}^h$ the surface traction on the traction boundary Γ^h. The computation of τ_{ij} in Eq. (3) involves hyper-elasticity using $\mathbf{F}^e$ in Eq. (1) and return-mapping algorithm in the principal stress space. The dependence of $a_{\Omega}(\mathbf{z},\bar{\mathbf{z}})$ on $\mathbf{z}$ is nonlinear from the elasto-plastic constitutive relation and nonlinear kinematics. The nonlinear variational Eq. (2) can be solved for displacement $\mathbf{z}$ iteratively using the Newton-Raphson method, which requires the linearization (Jacobian) of the structural energy form in Eq. (3) with respect to displacement increment $\Delta\mathbf{z}$ as

$$\begin{aligned} a^{*}_{\Omega}(\mathbf{z};\Delta\mathbf{z},\bar{\mathbf{z}}) = &\iint_{\Omega} \varepsilon_{ij}(\bar{\mathbf{z}})C^{alg}_{ijkl}\varepsilon_{kl}(\Delta\mathbf{z})\,d\Omega \\ &+\iint_{\Omega} \tau_{ij}\eta_{ij}(\Delta\mathbf{z},\bar{\mathbf{z}})\,d\Omega \end{aligned} \tag{5}$$

where C^{alg}_{ijkl} is the 4th-order consistent tangent stiffness tensor (see Simo, 1992) and $\tau_{ij}\eta_{ij}$ is the initial stiffness

term. Note that $a_\Omega^*(\mathbf{z};\Delta\mathbf{z},\bar{\mathbf{z}})$ is linear with respect to its arguments. Let the current time be t_n and the iteration counter be k+1, then the linearized incremental problem of Eq. (2) is

$$a_\Omega^*({}^n\mathbf{z}^k;\Delta\mathbf{z}^{k+1},\bar{\mathbf{z}}) = \ell_\Omega(\bar{\mathbf{z}}) - a_\Omega({}^n\mathbf{z}^k,\bar{\mathbf{z}}), \quad \forall\bar{\mathbf{z}}\in Z \tag{6}$$

The linear variational Eq. (6) is solved util the right side (residual force) vanishes, which means that the original nonlinear Eq. (2) is satisfied at t_n. After the solution is converged in Eq. (6), the plastic internal variables (back stress and effective plastic strain) are updated to the current configuration as well as $\mathbf{F}^p$ in Eq. (1).

Frictional Contact

A contact analysis is critical in simulation of the deep-drawing process that includes interactions between the workpiece and punch/die. Among the many contact formulations, the penalty regularization method is used in this paper, where a small penetration is allowed between the workpiece and rigid surface. Let Γ_C be the region where the workpiece is penetrating the rigid surface. Then this region is penalized by proportional to the amount of the penetration (g_n). The contact variational form is defined as

$$b_\Gamma(\mathbf{z},\bar{\mathbf{z}}) = \omega_n\int_{\Gamma_C} g_n\bar{\mathbf{z}}^T\mathbf{e}_n\,d\Gamma + \begin{cases} +\omega_t\int_{\Gamma_C} \nu g_t\bar{\mathbf{z}}^T\mathbf{e}_t\,d\Gamma, & \text{if } |\omega_t g_t| \le |\mu\omega_n g_n| \\ -\mu\omega_n\,\mathrm{sgn}(g_t)\int_{\Gamma_C}\nu g_n\bar{\mathbf{z}}^T\mathbf{e}_t\,d\Gamma, & \text{otherwise} \end{cases} \tag{7}$$

where ω_n and ω_t are the normal and tangential penalty parameters, $\mathbf{e}_n$ and $\mathbf{e}_t$ are the unit normal and tangent vector at the contact point, g_n and g_t are the normal gap and tangential slip, and μ is the frictional coefficient of Coulomb law. Note that Eq. (7) includes two conditions: the stick condition ($|\omega_t g_t| \le |\mu\omega_n g_n|$) where a microscopic-elastic motion exists between contact surfaces and the slip condition where a macroscopic-permanent motion exists. Using the stick condition, this is a regularized Coulomb friction model as shown in Fig. 1.

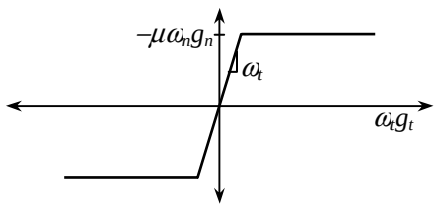

Fig. 1 Regularized Coulomb Friction Model

The contact variational form in Eq. (7) is nonlinear in displacement since variables g_n, g_t, $\mathbf{e}_n$, and $\mathbf{e}_t$ depend on the displacement implicitly and the contact region itself is not known *in priori*. The same linearization as the structural energy form in Eq. (5) can be carried out using the Newton-Raphson method. The linearized variational equation, including the frictional contact constraint, is

$$a_\Omega^*({}^n\mathbf{z}^k;\Delta\mathbf{z}^{k+1},\bar{\mathbf{z}}) + b_\Gamma^*({}^n\mathbf{z}^k;\Delta\mathbf{z}^{k+1},\bar{\mathbf{z}}) = \ell_\Omega(\bar{\mathbf{z}}) - a_\Omega({}^n\mathbf{z}^k,\bar{\mathbf{z}}) - b_\Gamma({}^n\mathbf{z}^k,\bar{\mathbf{z}}), \qquad \forall\bar{\mathbf{z}}\in Z \tag{8}$$

where $b_\Gamma^*(\mathbf{z};\Delta\mathbf{z},\bar{\mathbf{z}})$ is the linearized contact variational form obtained by linearization of Eq. (7). Detailed expression of $b_\Gamma^*(\mathbf{z};\Delta\mathbf{z},\bar{\mathbf{z}})$ can be found in Kim et al (1999) where two separate expressions of $b_\Gamma^*(\mathbf{z};\Delta\mathbf{z},\bar{\mathbf{z}})$ are derived for stick and slip conditions, respectively.

Meshfree Discretization and Nodal Integration

The continuum-based formulation of the structural problem in Eq. (8) has to be discretized in numerical approximation. The accuracy and stability of the solution critically depend on the numerical method employed. In this paper, a meshfree method (Liu, 1995) is used where the structural domain is discretized by a set of particle points. In the meshfree method, each particle point has a finite size of support that defines the domain of influence. Among the total number of particles *NP* in the domain, let *IP* be the number of particle points whose supports cover the point **X**. The state variable *z* is approximated as

$$z(\boldsymbol{X}) = \sum_{I=1}^{IP}\Psi_I(\boldsymbol{X})d_I \tag{9}$$

where $\Psi_I(\mathbf{X})$ is the *meshfree shape function* and d_I is the coefficient of approximation. $\Psi_I(\mathbf{X})$ is constructed to satisfy the completeness condition that Eq. (9) exactly approximates a certain order of polynomials. In the meshfree method, the smoothness of approximation is easily controlled by the order of kernel function (p-adaptivity). Since particles are not employed for the connectivity of the finite element, the imposition of more particles to the structure is easy (h-adaptivity). Unlike the finite element approximation, however, $\Psi_I(\mathbf{X})$ in Eq. (9) is a function of the global material point **x** and d_I is not the value of the displacement at node *I* in general, which requires more computational efforts than FEA.

The numerical integration of Eq. (8) is carried out using a nodal integration method (Chen et al, 2000) where the instability problem that exists in early development is resolved using a strain smoothening algorithm. Figure 2 shows a typical example of the domain partitioning

using the Voronoi diagram and the nodal volume (area) is used as a weight for the domain integration.

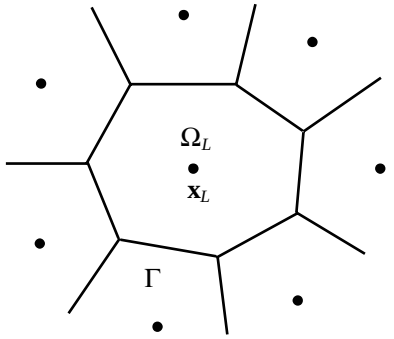

Fig. 2 Voronoi Diagram of the Scattered Particle Set

Using the approximation in Eq. (9) and numerical integration as explained in Fig. 1, the discretized variational equation is obtained, for given the Hilbert space $H^1(\Omega)$, as

$$\bar{\boldsymbol{d}}^T \boldsymbol{K}\, \boldsymbol{d} = \bar{\boldsymbol{d}}^T \boldsymbol{F}, \qquad \forall \bar{\boldsymbol{d}} \in H^1 \tag{10}$$

where **K** and **F** are the global tangent stiffness matrix and residual force vector, respectively. Since the variation of the generalized displacement $\mathbf{d} = [\mathbf{d}_1, \mathbf{d}_2, \ldots, \mathbf{d}_{NP}]^T$ is not nodal displacement, the imposition of the essential boundary condition is non-trivial in Eq. (10). Among the many proposed algorithms, the mixed boundary transformation method (Chen and Wang, 1999) is used in this paper to improve the efficiency of analysis while maintaining the accuracy of the solution.

3. DESIGN SENSITIVITY ANALYSIS

The DSA is to obtain derivative of the cost or performance measures with respect to design variables. In spite of some attractive features of the *adjoint variable method* in linear problems (Haug et al, 1986), it is very complicate and expensive to apply the adjoint variable method to the nonlinear path-dependent problems. Only the *direct differentiation method*, which is used in this paper, is applicable for general path dependent nonlinear problems.

The shape design is usually more effective than the sizing design. Since the design is the structural domain, each material point moves along the design direction. The material derivative concept in continuum mechanics is used to represent variation of the shape.

Shape Design of Elasto-plasticity

The classical theory of the shape DSA in linear problem is formally applied to nonlinear problems, since no mathematical proofs of the existence and uniqueness of design sensitivity are available. Since the configuration of the nonlinear problem is changed as analysis progresses, it is required to transform the current configuration to the initial geometry, where a design velocity field is defined, before taking material derivative with respect to the design.

The material derivative of the displacement vector can be expressed as a sum of the partial derivative and convective terms as

$$\dot{\boldsymbol{z}} = \boldsymbol{z}' + \nabla \boldsymbol{z} \boldsymbol{V} \tag{11}$$

where $\nabla = \partial/\partial \mathbf{X}$ is the gradient operator at the initial configuration and **V** is the design velocity vector, which represents the direction of design change. The direct differentiation method computes $\dot{\boldsymbol{z}}$ in Eq. (11) for given design velocity vector **V** as following. The material derivative of the variational equation Eq. (2) at the perturbed design can be taken, using Eq. (11), to obtain

$$a^*_\Omega(\boldsymbol{z}; \dot{\boldsymbol{z}}, \bar{\boldsymbol{z}}) = \ell'_V(\bar{\boldsymbol{z}}) - a'_V(\boldsymbol{z}, \bar{\boldsymbol{z}}), \qquad \forall \bar{\boldsymbol{z}} \in Z \tag{12}$$

where

$$\begin{aligned} a'_V(\boldsymbol{z}, \bar{\boldsymbol{z}}) = & \iint_\Omega \left(\bar{\varepsilon}_{ij} C^{alg}_{ijkl} \varepsilon^V_{kl} + \tau_{ij} \eta^V_{ij}(\boldsymbol{z}, \bar{\boldsymbol{z}}) + \tau_{ij} \bar{\varepsilon}_{ij} div \boldsymbol{V} \right) d\Omega \\ & + \iint_\Omega \left(\bar{\varepsilon}_{ij} C^{alg}_{ijkl} \varepsilon^p_{kl} + \tau_{ij} \eta^p_{ij}(\boldsymbol{z}, \bar{\boldsymbol{z}}) + \bar{\varepsilon}_{ij} \tau^{fic}_{ij} \right) d\Omega \end{aligned} \tag{13}$$

$$\begin{aligned} \ell'_V(\bar{\boldsymbol{z}}) \equiv & \iint_\Omega \left[\bar{\boldsymbol{z}}^T (\nabla \boldsymbol{f}^b \boldsymbol{V}) + \bar{\boldsymbol{z}}^T \boldsymbol{f}^b div \boldsymbol{V} \right] d\Omega \\ & + \int_{\Gamma^h} \left[\bar{\boldsymbol{z}}^T (\nabla \boldsymbol{f}^h \boldsymbol{V}) + \kappa \bar{\boldsymbol{z}}^T \boldsymbol{f}^h V_n) \right] d\Gamma \end{aligned} \tag{14}$$

are the structural and external load fictitious load forms, respectively. In Eq. (14), the applied load is assumed independent of deformation, i.e. conservative load and κ is the curvature of the traction boundary with normal component of design velocity V_n. The structural fictitious load in Eq. (13) contains explicitly dependent terms on design in the first integral and path dependent terms in the second integral. The path dependent terms include material derivatives of the internal plastic variables and intermediate configuration defined in Eq. (1).

Note that Eq. (12) has the same left side as the response analysis Eq. (6) if $\dot{\boldsymbol{z}}$ substituted by $\Delta \mathbf{z}$. Thus, the same tangent stiffness matrix **K**, which is already factorized, can be used for very efficient sensitivity computation. After solving the sensitivity Eq. (11) for $\dot{\boldsymbol{z}}$ up to the final configuration, the sensitivity of the performance measures can be calculated using the chain rule of differentiation.

Die Shape Design

The die shape DSA is to investigate the change of the response when the shape of the punch/die is changed. An optimized die shape design is very important for the manufacturing process, where usually a simple geometry of the workpiece is used to obtain a complicate final product using the punch/die shape. The shape of the die can be changed in a similar procedure as the shape design perturbation using the design velocity field on the punch/die geometry. The shape perturbation of the die affects the performance of the workpiece through the contact variational form in Eq. (7). By taking the material derivative of Eq. (7) and combining with the structural sensitivity Eq. (12), a linear variational equation is obtained as

$$\begin{aligned} &a_\Omega^*(\mathbf{z};\dot{\mathbf{z}},\bar{\mathbf{z}}) + b_\Gamma^*(\mathbf{z};\dot{\mathbf{z}},\bar{\mathbf{z}}) \\ &= \ell_V'(\bar{\mathbf{z}}) - a_V'(\mathbf{z},\bar{\mathbf{z}}) - b_V'(\mathbf{z},\bar{\mathbf{z}}), \quad \forall \bar{\mathbf{z}} \in Z \end{aligned} \tag{15}$$

where contact contribution of the fictitious load is denoted by $b_V'(\mathbf{z},\bar{\mathbf{z}})$. It is shown by Kim et al (1999) that the contact fictitious load $b_V'(\mathbf{z},\bar{\mathbf{z}})$ is path-independent for the frictionless contact problem and path-dependent for the fictional contact problem. Note that the design sensitivity Eq. (15) is linear although response analysis is nonlinear.

Meshfree Implementation

A major difference between finite element and meshfree methods is that the shape function of the meshfree approach depends on the coordinate of material points. Thus, for the material derivative of **z**,

$$\dot{\boldsymbol{z}}(\boldsymbol{X}) = \sum_{I=1}^{IP} \Psi_I(\boldsymbol{X})\dot{\boldsymbol{d}}_I + \sum_{I=1}^{IP} \dot{\Psi}_I(\boldsymbol{X})\boldsymbol{d}_I \tag{16}$$

The second term on the right of Eq. (16) a contribution from the dependence of the meshfree shape function on the shape design and can be obtained explicitly in terms of the design velocity vector **V**. Thus, for the structural fictitious load in Eq. (13), contributions from this second term needs to be accounted.

After following the same assembly procedure as structural analysis, the discretized design sensitivity equation is obtained as

$$\bar{\mathbf{d}}^{\mathrm{T}}\mathbf{K}\dot{\mathbf{d}} = \bar{\mathbf{d}}^{\mathrm{T}}(\mathbf{F}_\ell - \mathbf{F}_{\mathrm{a}} - \mathbf{F}_{\mathrm{b}}) \tag{17}$$

which can be solved for the material derivative of the generalized displacement. In Eq. (17), $\mathbf{F}_\ell$, $\mathbf{F}_{\mathrm{a}}$ and $\mathbf{F}_{\mathrm{b}}$ are fictitious loads contributed from the applied force, structural energy, and contact constraints, respectively. The sensitivity of the displacement can be obtained from Eq. (16). After solving Eq. (17) at the current time step, path-dependent variables have to be updated for the sensitivity computation at the next time step. The internal variables include the plastic evolution variables (effective plastic strain and back stress), the intermediate configuration that is defined by $\mathbf{F}^p$ in Eq. (1), and the displacement at the contact surface because of friction. After solving the design sensitivity equation up to the final configuration time, the sensitivity of the performance measure can be obtained using the chain rule of differentiation. Possible list of performance measures are the area of the workpiece, displacement, stress, back stress, effective plastic strain, contact force, drawing force through punch, and the shape difference between the desired and final geometry after spring-back.

4. DESIGN OPTIMIZATION

The design optimization of the deepdrawing process includes the parameterization of design, nonlinear meshfree analysis, shape DSA, and optimization algorithm. MSC/PATRAN is used as a tool of geometric modeling that uses a parametric representation. An efficient method of design velocity computation in the parametric space was proposed by Choi and Chang (1994). Very accurate and efficient sensitivity results are obtained to improve the convergence of optimization iteration.

Design Parameterization

Figure 3 shows analysis setting and design parameterization of the deepdrawing process. Only half of the model is solved using symmetric condition in the plane strain problem. The blank is modeled using 303 meshfree particles. The von Mises yield criterion is used with an isotropic hardening model. A constant friction coefficient is used in the modified Coulomb law. The draw die is fixed during punch motion stage while the blank holder exerts force against any motion of the blank. After maximum stroke of punch (30 mm), the punch, die, and blank holder are removed to calculate the amount of spring-back.

The first two parameters control the position of punch horizontally and vertically. Horizontal movement is very important since it controls the gap between punch and draw die. The third and fourth parameters are round radii of corners of the punch and draw die. A sharp corner may increase the plastic strain while reducing the amount of spring-back. The fifth parameter changes the thickness of the blank, which involves the shape change of the workpiece. The sixth parameter controls the gap between blank holder and die such that the frictional force on the blank can be changed.

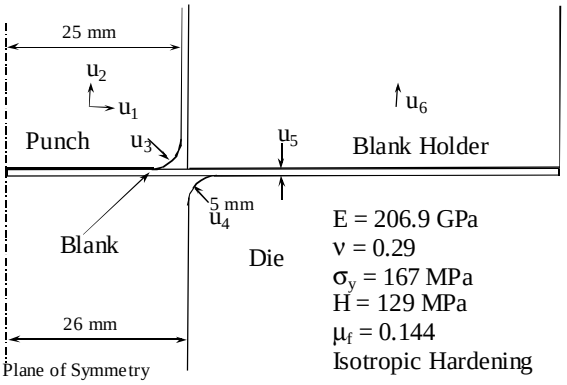

Fig. 3 Design Parameterization of Deepdrawing Process

Meshfree Nonlinear Analysis

Nonlinear meshfree analysis is carried out to simulate sping-back of the deepdrawing process. Rigid bodies are assumed for the punch, drawing die, and blank holder. Thus, numerical integration is involved only for the workpiece material. A displacement driven method is used such that the position of punch is given at each time step and converged configuration is found using the Newton-Raphson method. For the stress computation, an elastic predictor followed by a plastic return-mapping is used in the principal Kirchhoff stress. After finding a converged configuration, the factorized tangent stiffness matrix is stored to be used for DSA later.

A slave-master concept is used for the contact problem to impose the penalty regularization. The rigid surfaces (punch, draw die, and blank holder) are modeled as piecewise linear master segments. Using the linear discretization, a very simple expression of $b_\Gamma(\boldsymbol{z},\bar{\boldsymbol{z}})$ can be obtained since the unit normal and tangential vectors on the contact surface remain constant. However, there exists a possibility of the convergence problem at the kinked corner of adjacent linear master segmenets. A line search algorithm is used when that difficulty happens. The contact search is carried out for particles on the domain boundary. If a penetration into the rigid surface is detected, then a penalty is imposed using $b_\Gamma(\boldsymbol{z},\bar{\boldsymbol{z}})$ in Eq. (7). The stick/slip conditions are determined by measuring the amount of relative motion between two adjacent configurations.

Figure 4 shows the deformation history of the workpiece along with punch movement. Figure 5 shows the results of nonlinear analysis at the maximum deformation and after spring-back. Significant amount of material sliding is observed between the workpiece and draw die inspite of the existence of the friction. The spring-back occurs when the punch, draw die, and blank holder are removed. Although the amount of elastic spring-back is small at each part of the blank, the total displacement at the edge becomes significant because of the rotational effect.

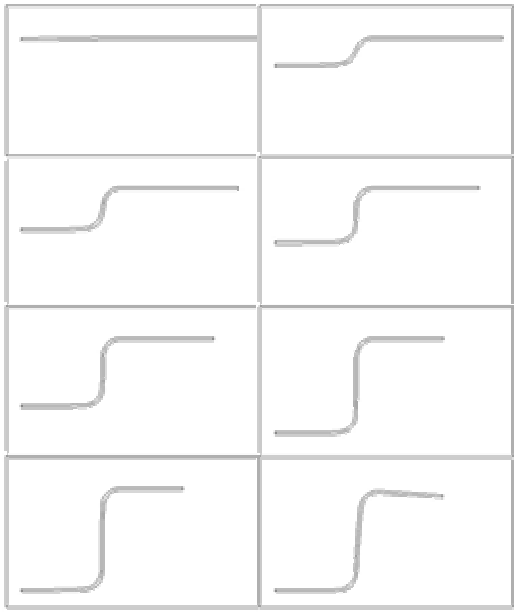

Fig. 4 Deformation History of the Workpiece

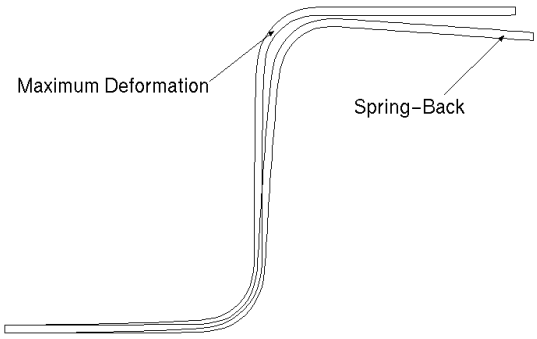

Fig. 5 Deepdrawing Analysis with Spring-Back

Figure 6 shows the contour plot of the effective plastic strain at the final configuration. High plastic strain distribution is observed around the vertical region. A design constraint is imposed for the maximum allowable plastic strain to prevent material failure due to excessive plastic deformation. In this paper the maximum allowable effective plastic strain is assumed to be 0.2.

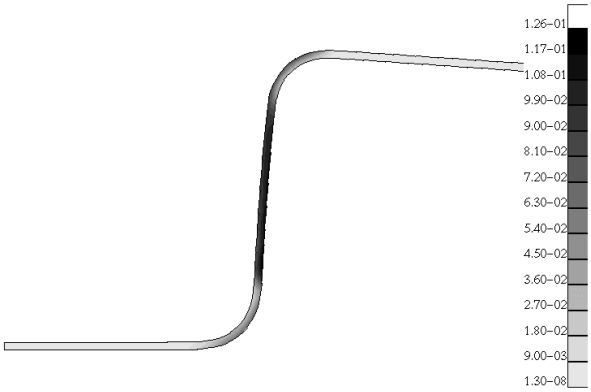

Fig. 6 Effective Plastic Strain Distribution

Sensitivity Analysis

Since there are six design parameters, design sensitivity Eq. (15) is solved six times at each converged load step. Thus, an efficient solver for the linear system of equations is very important for the computational cost. The performance measures are chosen for the effective plastic strain e^p and the shape difference G between the maximum deformation and after spring-back. Since the effective plastic strain is path-dependent variable and its sensitivity is updated at each configuration, no additional computation is required to compute sensitivity of e^p. The shape difference G is a function of material points at the final configuration. Thus, the sensitivity of G can be calculated using $\dot{\boldsymbol{z}}$ and the chain rule of differentiation as

$$\frac{d}{d\tau}[G(\boldsymbol{x})]\Big|_{\tau=0} = \frac{\partial G^T}{\partial \boldsymbol{x}}(\boldsymbol{V}+\dot{\boldsymbol{z}}) \tag{18}$$

The accuracy of DSA can be compared with the finite difference result by perturbing the design a small amount and solving the structural problem again. The finite difference method compute the sensitivity of the performance measure ψ by

$$\Delta\psi \approx \frac{\psi(\boldsymbol{x}+\Delta\tau\boldsymbol{V})-\psi(\boldsymbol{x})}{\Delta\tau} \tag{19}$$

for small $\Delta\tau$, which strongly depends on the accuracy of structural analysis and machine operation error.

The continuum-based design sensitivity method proposed in this paper yields very accurate and efficient results. Table 1 compares the accuracy of the proposed sensitivity ψ' of various performance measures and $\Delta\psi$ with excellent agreements. A very small perturbation $\Delta\tau = 10^{-6}$ is used for the finite difference results.

Table 1 Accuracy of Sensitivity Results

ψ	$\Delta\psi$	ψ'	$\Delta\psi/\psi'\times100$
u_1			
e^p_{41}	1.48092E-08	1.48111E-08	99.99
e^p_{45}	1.39025E-09	1.38995E-09	100.02
e^p_{50}	8.73928E-09	8.73917E-09	100.00
e^p_{55}	2.92573E-08	2.92558E-08	100.01
e^p_{142}	6.42704E-09	6.42645E-09	100.01
e^p_{147}	8.75082E-09	8.75167E-09	99.99
e^p_{152}	-4.88503E-08	-4.88486E-08	100.00
e^p_{157}	-2.08880E-08	-2.08875E-08	100.00
G	-4.31897E-05	-4.37835E-05	98.64
u_2			
e^p_{41}	-7.51065E-10	-8.28304E-10	90.68
e^p_{45}	-8.63393E-09	-8.77018E-09	98.45
e^p_{50}	-9.46012E-09	-9.42600E-09	100.36
e^p_{55}	-3.46566E-08	-3.32805E-08	104.13
e^p_{142}	-1.02204E-08	-1.02214E-08	99.99
e^p_{147}	2.30561E-09	2.27053E-09	101.55
e^p_{152}	5.58534E-08	5.58827E-08	99.95
e^p_{157}	2.49171E-08	2.41362E-08	103.24
G	2.51654E-05	2.57379E-05	97.78
u_3			
e^p_{41}	-1.81265E-09	-1.81292E-09	99.99
e^p_{45}	-8.32899E-10	-8.33645E-10	99.91
e^p_{50}	-4.11725E-09	-4.11707E-09	100.00
e^p_{55}	-1.60858E-08	-1.60891E-08	99.98
e^p_{142}	-4.17814E-09	-4.17970E-09	99.96
e^p_{147}	-8.43008E-10	-8.43061E-10	99.99
e^p_{152}	2.65440E-08	2.65487E-08	99.98
e^p_{157}	1.14224E-08	1.14229E-08	99.99
G	1.50596E-05	1.55745E-05	96.69
u_4			
e^p_{41}	-1.64206E-08	-1.64212E-08	100.00
e^p_{45}	-1.78461E-08	-1.78462E-08	100.00
e^p_{50}	-1.44561E-08	-1.44563E-08	100.00
e^p_{55}	-2.06306E-08	-2.06324E-08	99.99
e^p_{142}	5.10648E-09	5.10589E-09	100.01
e^p_{147}	-9.75899E-09	-9.75881E-09	100.00
e^p_{152}	-1.46721E-08	-1.46709E-08	100.01
e^p_{157}	-1.65305E-08	-1.65318E-08	99.99
G	5.16216E-05	5.47740E-05	94.24
u_5			
e^p_{41}	6.32293E-07	6.33335E-07	99.84
e^p_{45}	-3.42150E-07	-3.41924E-07	100.07
e^p_{50}	-1.48786E-07	-1.48986E-07	99.87
e^p_{55}	1.01051E-06	1.01077E-06	99.97
e^p_{142}	4.27720E-07	4.28280E-07	99.87
e^p_{147}	-6.64596E-07	-6.64791E-07	99.97
e^p_{152}	-2.43935E-06	-2.43989E-06	99.98
e^p_{157}	-1.54750E-06	-1.54754E-06	100.00
G	-8.01735E-04	-8.51401E-04	94.17
u_6			
e^p_{41}	5.21628E-07	5.22109E-07	99.91
e^p_{45}	-2.04683E-07	-2.05656E-07	99.53
e^p_{50}	4.05362E-08	3.54155E-08	114.46
e^p_{55}	1.20942E-06	1.20331E-06	100.51
e^p_{142}	4.41449E-07	4.42033E-07	99.87
e^p_{147}	-5.38989E-07	-5.39373E-07	99.93
e^p_{152}	-2.39527E-06	-2.39169E-06	100.15
e^p_{157}	-1.42736E-06	-1.42780E-06	99.97
G	-1.19663E-03	-1.25937E-03	95.02

In Table 1, the design sensitivity of the performance G does not agree as much as other performance measures. The reason is that the magnitude of the performance change is larger compared to other performance measures. For example, G is changed 10^3 times larger than other performance measures for u_6. Thus, the finite difference approximation in Eq. (19) contains an error in approximation. This will be improved if the magnitude of the design perturbation is decreased, which may cause inaccuracy of other performance measures caused by numerical errors. Thus, it is very difficult to choose an appropriate perturbation size for the finite difference method.

The cost of nonlinear meshfree analysis to solve the deepdrawing problem in Fig. 5 is 8,082 sec in HP exemplar workstation, whereas DSA requires 1,843 sec for six design parameters, which is corresponding to 3.8% of the analysis cost per design parameter. This efficiency is expected since sensitivity analysis uses already factorized tangent stiffness matrix and no iteration is required for sensitivity computation.

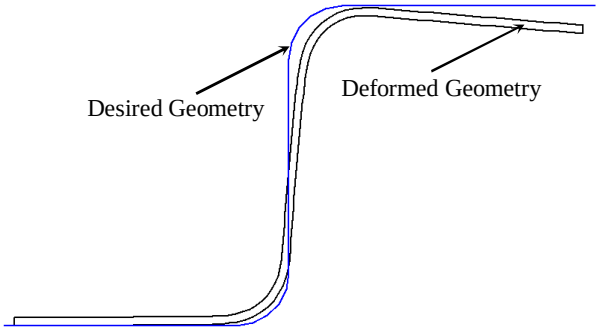

Fig. 7 Shape Difference Between Deformed Geometry and Desired Geometry

Design Optimization

The design optimization problem is formulated to

$$\begin{aligned} \text{minimize} \quad & G = \sum (P(\boldsymbol{x}_i) - \boldsymbol{x}_i)^2 \\ \text{subject to} \quad & e^p \le 0.2 \\ & t_i \ge 0.6 \\ & -0.1 \le u_1 \le 0.1 \\ & -0.01 \le u_2 \le 0.1 \\ & -1.1 \le u_3 \le 1.1 \\ & -1.1 \le u_4 \le 1.1 \\ & -0.01 \le u_5 \le 0.01 \\ & -0.02 \le u_6 \le 0.1 \end{aligned} \tag{20}$$

where $P(\mathbf{x})$ is the orthogonally projected position of the particle point $\mathbf{x}$ onto the desired final shape of the workpiece. Figure 7 shows the difference between the desired geometry and deformed geometry after spring-back. The design constraints are imposed to limit the magnitude of the effective plastic strain, which may cause material failure or severe necking. In addition, the minimum thickness of the each section is limited. Limits on u_i are established based on the geometry of the problem and kinematics. Since u_i's represent the relative movements of the geometry, the initial values set to zero.

The design optimization problem is solved using the sequential quadratic programming method in DOT (Vanderplaats, 1997) by supplying meshfree analysis results and design sensitivity information. At each iteration, the initial geometry of the problem is updated.

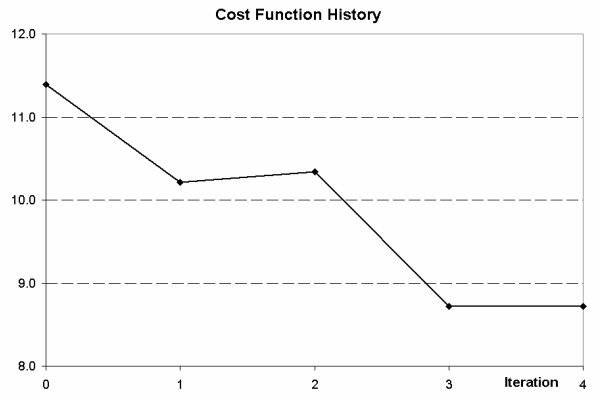

(a) Cost Function History

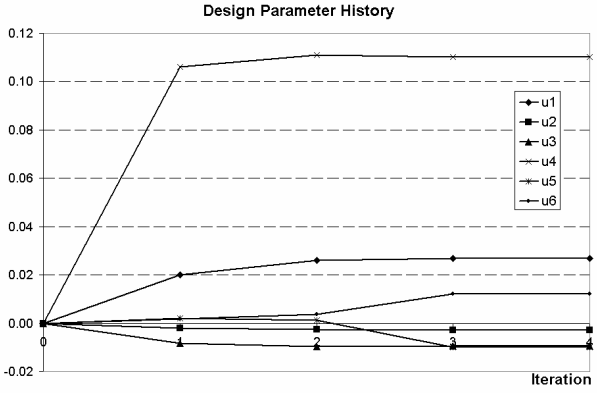

(b) Design Parameter History

Fig. 8 Deepdrawing Optimization History

The design optimization problem is converged in four iterations, which is quite fast convergence considering nonlinearity involved in structural analysis. Figure 8(a) shows the history of cost function G during optimization. The cost function, which is the spring-back

amount, is reduced up to 24% of the initial design. All constraints are satisfied with no active constraint at the optimum design. Fig. 8(b) shows the history of design parameters. The corner radius (u_4) of rigid die is increased significantly to reduce over-deflection of workpiece at the binder part. The corner radius (u_3) of punch is decreased to make the workpiece vertical. It is interesting to note that the binder force, which is controlled by u_6, is decreased from the initial design, which in turn reduces the frictional force.

The deformed shapes of the initial and optimum designs are shown in Figure 9. Over-deflection of the initial design around blank holder area is improved significantly to match the desired shape shown in Fig. 7. The vertical slope is also improved compared to the initial design. However, it turns out that making 90 degree vertical slop is very difficult based on the current manufacturing process unless a spring-forward method is used, which is not possible for this deepdrawing process. Note that the radius of bottom corner is increased in the optimum design. However, an effort to fit this region will cause bigger deviation from the desired shape in other regions.

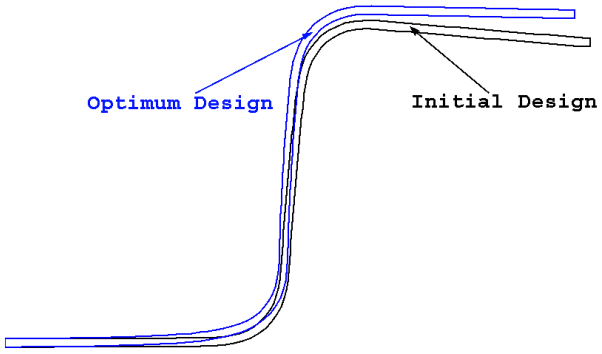

Fig. 9 Final Deformed Shapes of Initial and Optimum Designs After Spring-Back

Figure 10 compares the distributions of effective plastic strains of the initial and optimum designs. The maximum value of effective plastic strain at optimum design is reduced about 12% from that of the initial design. It is interesting to note that the amount of spring-back is reduced while the plastic deformation is decreased.

In the deepdrawing process, a necking phenomenon is an important criterion to determine the quality of the product and necking amount is proportional to the plastic deformation. In this paper, necking is measured by the thickness reduction along the edge of the blank. Figure 11 shows the thickness reductions of the initial and optimum designs. It is clear that the optimum design shows less plastic deformation compared to the initial design, which is consistent with effective plastic strain distribution in Fig.10. Since the plastic deformation is volume conserving, the area of the graph is transformed into the increase of cord length of the blank. The area of initial design in Fig. 11 is 1.18mm^2 and 0.716 mm^2 for the optimum design.

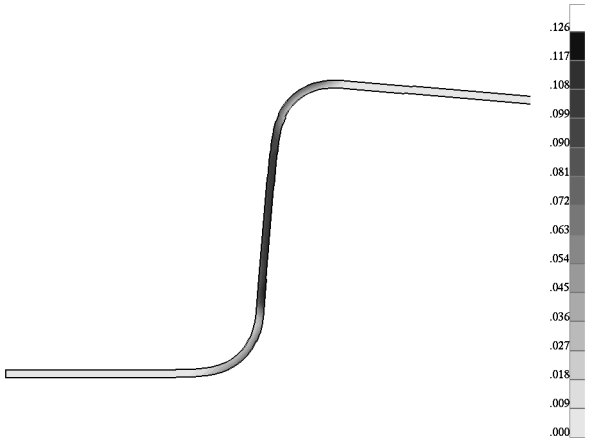

(a) Initial Design

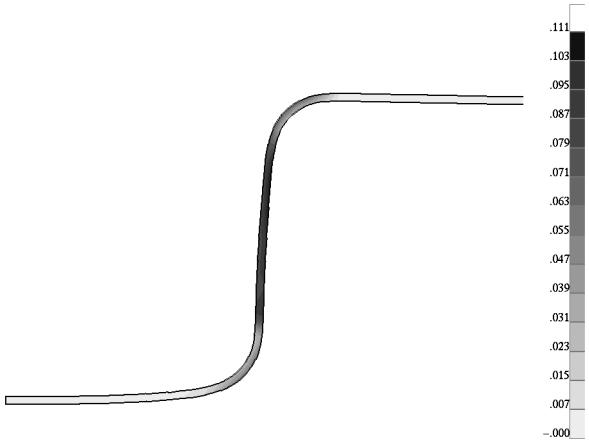

(b) Optimum Design

Fig. 10 Effective Plastic Strain Distributions

Initial cord length 75mm of the blank is stretched during simulation to 76.46mm, while the total cord length is 75.87mm at optimum design, which is consistent with the reduction of plastic deformation at the optimum design. These amounts of stretches show consistent results of the areas in Fig. 11.

5. CONCLUSION

Very efficient and accurate methods of numerical simulation and design sensitivity analysis methods for a metal stamping manufacturing process design are proposed using meshfree nonlinear analysis and material

derivative approach. The design optimum result shows the feasibility of the proposed method for a difficult deepdrawing process.

In this paper, the shapes of the workpiece and rigid surfaces, and binding force are considered for design parameters.

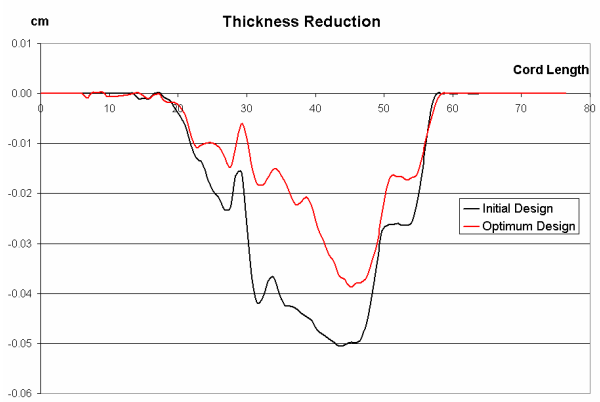

Fig. 11 Thickness Reduction of Workpiece

ACKNOWLEDGEMENT

This research is supported by NSF/DARPA Optimized Portable Algorithms and Application Libraries (OPAAL). The support is gratefully acknowledged.

REFERENCE

Antunez. H.J. and Kleiber, M. (1996), Sensitivity of forming processes to shape parameters, *Comput. Methods Appl. Mech. Eng*. **137**, 189-206

Badrinarayanan, S. and Zabaras, N. (1996), A sensitivity analysis for the optimal design of metal-forming processes, *Comput. Methods Appl. Mech. Eng.* **129**, 319-348

Balagangadhar, D. and Tortorelli, D.A. (1998), Design and analysis of large deformation continuous elastoplastic manufacturing processes via a steady displacement-based formulation, *7th AIAA/USAF/NASA/ ISSMO Symposium on Multidisciplinary Analysis and Optimization*, St. Louise, MO, 1396-1406

Choi, K.K. and Chang, K.H. (1994), A study of design velocity field computation for shape optimal design, *Finite Elements in Analysis and Design*, **15**, 317-341.

Chen, J.S., Pan, C., Roque, C.M.D.L., and Wang, H.P. (1998), A Lagrangian reproducing kernel particle method for metal forming analysis, *Comp. Mech.* **22**, 289-307 (1998)

Chen, J.S., Wu, C.T., Yoon, S., and You, Y. (1999), Stabilized conforming nodal integration for Galerkin meshfree methods, submitted, *Int. J. Num. Methods Eng*.

Chen, J.S. and Wang, H.P. (1999), New boundary condition treatments for meshless computation of contact problems, in press, *Comput. Methods Appl. Mech. Eng.*

Chung, S.H. and Hwang, S.M. (1998), Optimal process design in non-isothermal, non-steady metal forming by the finite element method, *Int. J. Num. Methods Eng.* **42**, 1343-1390

Haug, E.J., Choi, K.K., and Komkov, V. (1986), *Design sensitivity analysis of structural systems*, Academic Press, NY

Kim, N.H., Choi, K.K., and Chen, J.S. (1999), Shape design sensitivity analysis and optimization of elastoplasticity with frictional contact, to appear, *AIAA J*.

Lee, E.H. (1969), Elastic-plastic deformation at finite strains, *J. Appl. Mech*. **36**, 1-6

Liu, W.K., Jun, S., and Zhang, Y.F. (1995), Reproducing kernel particle methods, *Int. J. Num. Methods in Fluids* **20**, 1081-1106

Maniatty, A.M. and Chen, M.F. (1996), Shape sensitivity analysis for steady metal-forming processes, *Int. J. Num. Methods Eng*. **39**, 1199-1217

Simo, J.C. (1992), Algorithms for static and dynamic multiplicative plasticity that preserve the classical return mapping schemes of the infinitesimal theory, *Comput. Methods Appl. Mech. Eng.* **99**, 61-112

Vanderplaats, G.N. (1997), *DOT User's Manual*, VMA Corp.

Wiechmann, W. and Barthold, F.J. (1998), Remarks on variational design sensitivity analysis of structures with large elastoplastic deformations, 7th AIAA/USAF/ NASA/ISSMO Symposium on Multidisciplinary Analysis and Optimization, St. Louise, MO, 349-358

Zhao, G.Q., Wright, E., and Grandhi, R.V. (1997), Preform die shape design in metal forming using an optimization method, *Int. J. Num. Methods Eng.* **40**, 1213-1230